Development 137, 3449-3458 (2010) doi:10.1242/dev.045310


# Integrin αV is necessary for gastrulation movements that regulate vertebrate body asymmetry

**Ararat J. Ablooglu*, Eugene Tkachenko, Jian Kang and Sanford J. Shattil**

## SUMMARY

Integrin αV can form heterodimers with several β subunits to mediate cell-cell and cell-extracellular matrix interactions. During zebrafish gastrulation, *αV* is expressed maternally and zygotically. Here, we used a morpholino-mediated *αV* knockdown strategy to study αV function. Although *αV* morphants displayed vascular defects, they also exhibited left-right body asymmetry defects affecting multiple visceral organs. This was preceded by mislocalization of dorsal forerunner cells (DFCs) and malformation of the Kupffer's vesicle (KV) laterality organ. These defects were rescued with morpholino-resistant *αV* mRNA. Like *αV*, integrin *β1b* was expressed in DFCs, and *β1b* knockdown largely recapitulated the laterality phenotype of *αV* morphants. When tracked in real-time, individual DFCs of both morphants showed defects in DFC migration, preventing them from organizing into a KV of normal shape and size. Thus, we propose that αVβ1b mediates cellular interactions that are necessary for DFC clustering and movements necessary for Kupffer's vesicle formation, uncovering an early contribution of integrins to the regulation of vertebrate laterality.

**KEY WORDS: Alpha V, Beta 1b, Dorsal forerunner cells, Gastrulation, Integrin, Zebrafish**

## INTRODUCTION

Integrins mediate cell-cell and cell-extracellular matrix (ECM) interactions. The eighteen α and eight β integrin subunits in mammals can assemble into 24 different αβ heterodimers (Hynes, 2002). Specific integrins recognize a restricted range of ECM ligands (Plow et al., 2000; Wendel et al., 1998), and integrin affinity for these ligands is controlled by 'inside-out' signaling pathways that converge upon the integrin cytoplasmic and transmembrane domains to activate the extracellular domains. Ligand binding to integrin triggers 'outside-in' signals that mediate anchorage-dependent events, including cell migration, proliferation, differentiation and survival (Hynes, 2002; Luo et al., 2007).

In mammals, the αV integrin subunit can associate with any of five β subunits (β1, β3, β5, β6 or β8) and αV integrins typically recognize Arg-Gly-Asp-containing ligands, such as fibronectin, vitronectin, osteopontin and latency-associated peptide-TGF1β (Hynes, 2002; Takada et al., 2007). Postnatally, αV integrins have been implicated in cellular responses to injury, immunity, angiogenesis and aspects of tumor progression (Nemeth et al., 2007; Takada et al., 2007). During vertebrate development, αV integrins exhibit a wide distribution of overlapping expression domains in mammalian, avian and zebrafish embryos (Ablooglu et al., 2007; Delannet et al., 1994; Neugebauer et al., 1991; Testaz et al., 1999; Yamada et al., 1995). The developmental importance of αV is illustrated by the phenotype of *αV* (*itgav* – Zebrafish Information Network) knockout mice, which demonstrate improper formation of embryonic cerebral blood vessels and defective axon and glia interactions in the postnatal central nervous system (Bader et al., 1998; McCarty et al., 2005; McCarty et al., 2002). However, as αV is maternally deposited in mice (Sutherland et al., 1993) and up to 20% of αV-null mice survive to birth (Bader et al., 1998), the opportunity to uncover potential roles for αV in very early mouse development has been limited.

Here, we used antisense morpholino oligonucleotides (MOs) to transiently knockdown integrin αV in zebrafish (Eisen and Smith, 2008; Nasevicius and Ekker, 2000). We provide the first evidence that depletion of αV, along with depletion of one of its potential β subunit partners, β1b, leads to defective dorsal forerunner cell (DFC) migration during gastrulation. Recent reports have shown that DFC migration is important for the formation of Kupffer's vesicle (KV), a ciliated organ involved in left-right body axis specification in zebrafish (Amack et al., 2007; Amack and Yost, 2004; Essner et al., 2005; Essner et al., 2002; Oishi et al., 2006; Schneider et al., 2008). Indeed, we find that KV is abnormally formed in αV and β1b morphants and that both exhibit body asymmetry defects later in development.

## MATERIALS AND METHODS

### Zebrafish maintenance and stocks

Wild-type *Danio rerio* and *Tg[sox17:gGFP]* embryos were raised at 28.5°C. Embryos from natural matings were kept in 1-phenyl-2-thiourea (PTU; 0.003%) to inhibit pigmentation and staged according to Kimmel et al. (Kimmel et al., 1995). Zebrafish were housed in the UCSD animal facility and experiments were performed in accordance with the guidelines of UCSD Institutional Animal Care and Use Committee.

### Antisense depletion of integrins αV and βb

MOs used (see Figs S1 and S5 in the supplementary material) were: *αV1*, 5′-AGTGTTTGCCCATGTTTTGAGTCTC-3′; *αV2*, 5′-AGTAGATGG-AGATCGCGCTGTTTGT-3′; *αVEI10*, 5′-GTCAGTGCAAATCATT-ACTCACCCA-3′; *αV1miss* (mutated residues in lower case), 5′-AcTcTTTcCCgATcTTTTcAGTgTC-3′; standard control MO, 5′-CCTCTTACCTCAGTTACAATTTATA-3′; *β1b1*, 5′-GGAGCAGCCTTA-CGTCCATCTTAAC-3′; *β1bEI10*, 5′-GCCAGTTTGAGTGAATAAC-TCACCT-3′. All MOs were obtained from Gene Tools (Philomath, OR, USA). MOs were injected at the 1- to 4-cell-stage blastulae except where

Department of Medicine, University of California San Diego, La Jolla, CA 92093-0726, USA.

*Author for correspondence (aablooglu@ucsd.edu)

**Accepted 6 August 2010**

noted. The impact of exon-intron-specific MOs on splicing was determined by RT-PCR with RNAs extracted from 3-6 somite stage (SS) AB embryos using the following primers (forward, backward, targeted exons, PCR fragment size): αV, 5′-GTTATTTGGGTTACTCTGTGGCTGTT-3′, 5′-GTTTGATGACACTGTTGAAGGTGAAGC-3′, exons 7 and 11, 336 bp; β1b, 5′-GCTCCAACATCTCCATTGGGGACGA-3′, and 5′-CAGATGTCAGTGCCATTATCCATAC-3′, exons 9 and 11, 334 bp. The altered splicing events were identified by size and DNA sequencing: α*VEI10* MO resulted in a deletion of exon 10, yielding a 283 bp fragment; β*1bEI10* MO caused an insertion of intron 10, yielding a 409 bp fragment.

### mRNA injections

Zebrafish α*V* mRNA (*mαV* RNA) was synthesized with mMESSAGE mMACHINE T7 Ultra Kit (Ambion, Austin, TX, USA). The 5′ UTR of α*V* cDNA was altered and missense and silent mutations were introduced to prevent and reduce possible α*V1* interactions at its recognition site (mutated residues in lower case, start codon in parenthesis): 5′-agtggcggccgC(ATG)GGgAAgCAtT-3′. The resulting cDNA did not retain the α*V2* segment (see Fig. S1 in the supplementary material). For MO rescue experiments, 200 pg of capped RNA was co-injected with 1.25 ng α*V1* or 1.75 ng α*V2* at the 1- to 4-cell-stage blastulae.

### Recombinant zebrafish integrin αV protein generation and antibody production

An N-terminal His-tagged 813 bp fragment of zebrafish αV cDNA, resulting a 34.2 kDa recombinant protein, coding for amino acid residues His106 to Leu376, was bacterially expressed and purified with Ni-NTA agarose beads (QIAGEN, Valencia, CA, USA). Approximately 1 mg of recombinant protein was used for immunization of rabbits (ab18001, Millipore, Temecula, CA, USA).

### Cell culture, protein analysis and western blotting

General methods for cell culture, protein analysis and western blotting were similar to Ablooglu et al. (Ablooglu et al., 2007). The antigen specificity of rabbit serum raised against recombinant zebrafish αV was tested in cell culture assays. A total of 20 μg CHO cell lysates or total zebrafish embryonic lysates from 5-8 SS embryos were resolved on 7.5% SDS-PAGE and analyzed by western blotting with the following antibodies: rabbit anti-zebrafish αV (ab18001, Millipore, Temecula, CA, USA) and β-actin antibody (ab6276, Abcam, Cambridge, MA, USA). Immunoreactive signals were detected and quantified by infrared emission spectrometry (Odyssey, Li-Cor Biosciences, Lincoln, NE, USA).

### WISH analysis

General methods for WISH were similar to Ablooglu et al. (Ablooglu et al., 2007). Standard molecular cloning techniques were used to prepare antisense riboprobes and their GenBank accession numbers are as follows: *cas*, AF362749; *ntl*, NM_131162; *sox17*, NM_131287; *spaw*, NM_180967; *vtn*, NM_001139461; *pdx1*, NM_131443.

### Immunohistochemistry and image analysis

Paraformaldehyde-fixed (4%) embryos were kept in methanol and rehydrated in incubation buffer containing 1× PBS, 0.5% Triton X-100, 5% BSA and 2% goat serum. The primary antibodies were used at 1:200 dilution: mouse anti-acetylated tubulin (T-6793, Sigma, St Louis, MO, USA); rabbit anti-aPKC-ζ (sc-216, Santa Cruz Biotechnology Inc., CA, USA); mouse anti-ZO-1 (339100, Invitrogen, Carlsbad, CA, USA). The secondary antibodies were used at 1:500 dilution: goat anti-mouse IgG (H+L) Alexa-Fluor 488 (A11017, Invitrogen, Carlsbad, CA, USA); goat anti-mouse IgG (H+L) Alexa-Fluor (A11031, Invitrogen); goat anti-mouse IgG (H+L) Alexa-Fluor 647 (A21237, Invitrogen); goat anti-rabbit IgG (H+L) Alexa-Fluor 568 (A11011, Invitrogen). Deyolked and Hoechst-stained (1:5000, Invitrogen) embryos were transferred into 50% glycerol.

Methods to determine individual DFC orientation and length-width ratio measurements were similar to previous studies (Davidson et al., 2006; Ezin et al., 2006). Half-rose diagrams were generated in six sectors with 30 degree (θ) intervals, representing anterior (a) with 0 θ, mediolateral axis (ml) with 90 θ and posterior (p) with 180 θ. Individual DFC length (L), the longest axis, and width (W), the widest distance across the DFC that is perpendicular to the length, were used to establish L-W ratios. Confocal images were captured with a Nikon Eclipse 80i microscope with a 40× objective, or with an Olympus FV1000 with a 20× objective. Multiple focal-plane confocal images of KV were acquired at 0.3 μm step-size *z*-series and of DFCs at 1 μm step-size *z*-series. 3D or 4D immunofluorescence images were assembled using Volocity 5.2.0 (Improvision, MA, USA), ImageJ (NIH) and Photoshop (Adobe) software. All images were examined in blind and analyzed by both ANOVA as a group and by Student's *t*-test. From the confocal images of *Tg(sox17:GFP)* embryos, we were able to identify 49-60% of individual DFC boundaries per morphant per embryo, percentages significant enough ($P<0.05$) to assume they are representative of the entire DFC population (Cochran, 1977).

### Live imaging

In order to visualize DFC migration and individual DFC shape in vivo, 1- to 4-cell-stage blastomeres of *Tg(sox17:GFP)* embryos were injected either with MOs alone or with BODIPY TR ceramide (B-34400, Invitrogen) to outline cellular boundaries. Embryos were manually dechorionated and used for time-lapse, multiple focal plane 2 μm step-size *z*-series (4D) microscopy at 24°C. A method to detect the cell-cluster edge was adapted from Machacek and Danuser (Machacek and Danuser, 2006) and, instead of individual cell edge detection, we identified uniform multicellular DFC cluster edges. Unlike α*V1miss* control morphants, DFCs in α*V1* and β*1bEI10* morphants were not clustered homogeneously and had fewer cell-cell contacts, with visible gaps, and often formed multiple DFC clusters (compare Movies 1 and 2 versus 3-6 in the supplementary material). In these instances we identified smaller GFP-positive DFC clusters that remained as clustered during the length of imaging (e.g. α*V1* in Fig. 5B). Individual cells that did not form a DFC cluster and migrated in all three axes were excluded from migration analyses. Velocity maps were calculated by finite differences of positions in consecutive frame triplets at T–1, T and T+1. Large protrusions were analyzed as previously described (Davidson et al., 2006), where each large and distinct protrusion was manually tracked and its appearance-disappearance cycle confirmed during the recorded time-lapse sequence.

## RESULTS

### Integrin αV is necessary for proper left-right patterning in zebrafish embryos

Gene knockdown in zebrafish can be accomplished with translation-blocking or splice-inhibiting antisense MOs (Eisen and Smith, 2008; Nasevicius and Ekker, 2000). The former interfere with translation of both maternal and zygotic transcripts, whereas the latter interfere primarily with unspliced zygotic transcripts (Abrams and Mullins, 2009; Eisen and Smith, 2008; Nasevicius and Ekker, 2000). Translation-blocking MOs (α*V1*, α*V2*) were designed to target the AUG start site within the α*V* 5′UTR (see Fig. S1 in the supplementary material). The efficacy of α*V1* in knocking down αV was determined on western blots of embryo lysates probed with an αV-specific antibody. In addition, we also used a splice-inhibiting MO (α*VEI10*) designed to yield a nonfunctional protein, and its efficacy was confirmed by RT-PCR (see Fig. S1 in the supplementary material).

As αV knockout mice exhibit myocardial abnormalities (Bader et al., 1998) and one of the earliest gross phenotypic abnormalities in α*V1* morphants was abnormal heart development and pericardial edema (see below), we focused first on heart tube formation (Fig. 1A-D). As expected, the heart tube was on the left side of the body in the vast majority (83.8±3.8%, $n=567$) of embryos injected with the standard control MO (Fig. 1E; see Table S1 in the supplementary material). By contrast, this pattern was reversed in α*V1* morphants, with the heart tube on the left in only 47.6±4.0% of embryos ($n=569$). When embryos were co-injected with α*V1* and morpholino-resistant *mαV* RNA, the α*V1* morphant phenotype

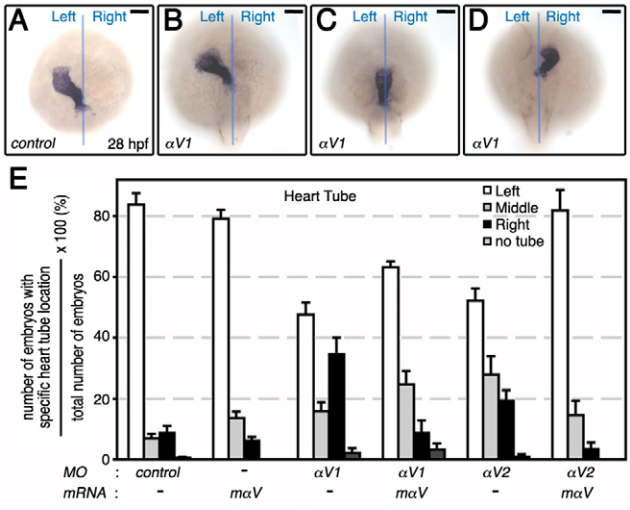


**Fig. 1. Integrin αV knockdown perturbs proper heart tube asymmetry in zebrafish embryos.** (**A-D**) Dorsal views of 28 hours post-fertilization (hpf) embryos hybridized with a probe to *cmlc2* to determine heart tube location. Scale bars: 100 μm. (A) Embryo injected with standard control MO. (B-D) Embryos injected with α*V1*. (**E**) Bar graphs showing effects of αV integrin loss of function on heart tube location. Data expressed as number of embryos with *cmlc2* expression location divided by total number of embryos used per experiment × 100 (%) ± s.e.m. See also Table S1 in the supplementary material.

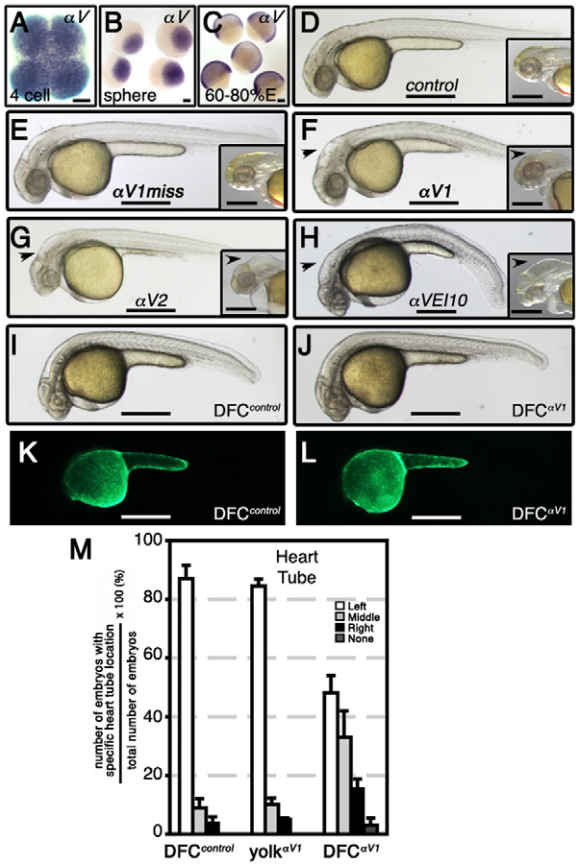


**Fig. 2. Integrin αV mRNA is a maternal factor and its specific knockdown in DFCs alters heart tube asymmetry.** (**A-C**) WISH analysis in wild-type zebrafish embryos shows maternal expression of α*V* at the 4-cell stage (A) and sphere stage (4 hpf; B), and zygotic expression at 60-80% epiboly (E). (**D-L**) Lateral views of live embryos at 32 hpf (D-H) or 28 hpf (I-L). When integrin αV morpholinos (MOs) were delivered at the 1- to 4-cell stage, morphants developed hydrocephaly in the fourth ventricle (black arrowheads) that was also associated with formation of abnormal cerebellum. Control (D) and α*V1miss* (E) morphants had wild-type head phenotype. Insets in panels D to H represent ~55 hpf head phenotype of respective morphants. Note intracerebral bleeding (pink color behind eyes) at 55 hpf. When control or α*V1* MOs were injected into yolk at mid-blastula stage (512-1000 cells), which targets DFCs specifically, these animals had wild-type phenotype (I,J). (K,L) Fluorescence images corresponding to I and J, revealing that MOs were exclusively present in the yolk cell. (**M**) Bar graph showing the effects of αV integrin loss-of-function specifically in DFCs on heart tube location. Data expressed are similar to those in Fig. 1E. Scale bars: 100 μm in A-C; 500 μm in D-L. See also Table S3 in the supplementary material.

was partially reversed (63.2±1.9% left, *n*=224), suggesting that the effects of α*V1* were specific. This heart tube phenotype was also induced with a second translation-blocking MO (α*V2*), and it too was partially reversed by co-injection of *mαV* RNA (Fig. 1E; see Table S1 in the supplementary material).

To further assess the consequences of αV loss-of-function on left-right patterning, we examined expression of the earliest known asymmetric marker *spaw* in the anterior lateral plate mesoderm (LPM) (Long et al., 2003), *lft2* in the left heart primordia (Amack and Yost, 2004), *vtn* in the liver (Thisse et al., 2004) and *pdx1* in the pancreatic bud (Ober et al., 2003) (see Fig. S2 in the supplementary material). Compared with embryos injected with control MOs, α*V* morphants displayed randomized left-right gene expression profiles, with partial rescue of each defect by co-injection of *mαV* mRNA (see Fig. S2 and Table S2 in the supplementary material).

α*V* transcripts are widely present in gastrulating embryos (Fig. 2A-C) and are selectively localized in developing notochord at the beginning of segmentation (Ablooglu et al., 2007). As defective midline structures are known to cause laterality defects (Bisgrove et al., 2000), one potential explanation for our results is a compromise in the integrity of midline structures. However, αV1 morphants exhibited intact, *ntl*-positive notochords (see Fig. S3 in the supplementary material), arguing against this possibility.

## αV is required for dorsal forerunner cell function

Given the central role of KV in specifying laterality in zebrafish (Essner et al., 2005), our attention then focused on DFCs, which migrate at the leading edge of the dorsal blastoderm margin (Cooper and D'Amico, 1996; Oteiza et al., 2008) and are precursors of KV. Specifically, we wondered if α*V* might be present in DFCs and required for its function during gastrulation. Although maternal (Fig. 2A) and zygotic (Fig. 2B,C) expression profiles suggested that α*V* mRNA, and possibly αV protein, is present in DFCs, we chose a more direct and functional assay to generate DFC-selective morphants (DFC$^{αV1}$), which were created by injecting α*V1* MO into the yolk cell at mid-blastula stage (Amack and Yost, 2004).

Unlike standard control MO and α*V1miss*-injected morphants (Fig. 2D,E), when α*V1*, α*V2* or α*VEI10* MOs were delivered at the 1-4 cell stage, α*V* morphants exhibited abnormal cerebellum, hydrocephaly involving the fourth ventricle, and pericardial edema (Fig. 2F-H). Although DFC$^{αV1}$ morphants were grossly similar to

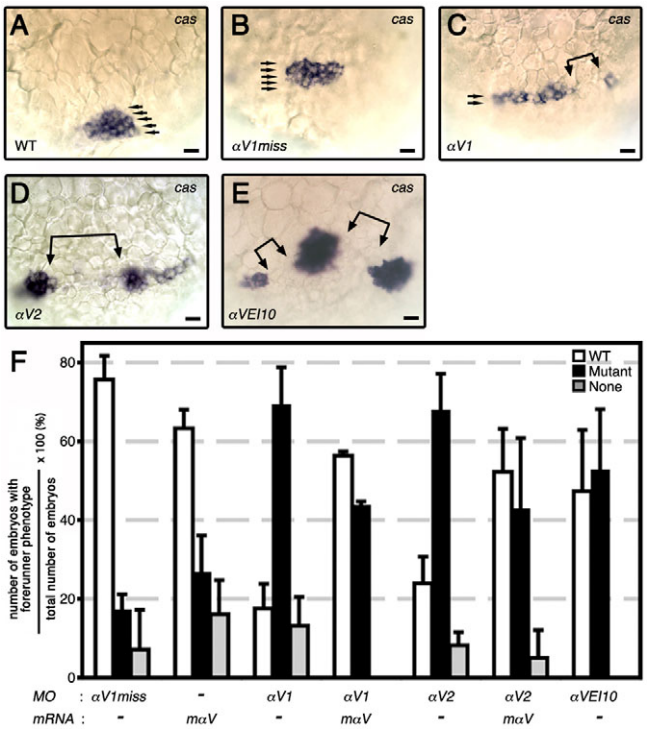


**Fig. 3. Migratory DFCs are not properly formed in αV morphants.** (**A-E**) Dorsal views of MO-injected embryos were slightly tilted to visualize *cas* expression (arrows, black) in DFCs at 80% E. Gaps in DFC field are indicated with bracketed arrows. (**F**) Bar graph showing scores from DFC phenotypes. Phenotypic classification of DFCs were as follows: Wild-type (WT), ovoid DFC cluster; mutant, a linear array of DFCs with occasional gaps; none, no visible DFCs. Data expressed are similar to those in Fig. 1E. Scale bars: 20 μm. See also Table S4 in the supplementary material.

wild-type embryos (Fig. 2I-L), their heart tube location was randomized compared with controls (DFC$^{\alpha V1}$, 48.2±5.9% left, *n*=223; DFC$^{control}$, 87.0±4.5% left, *n*=251) (Fig. 2M; see Table S3 in the supplementary material). However, when α*V1* was delivered into the yolk cell at an even later stage [dome stage to 30% epiboly (30% E)], when DFC connections with yolk cells are considered to be closed (D'Amico and Cooper, 1997; Essner et al., 2005), these yolk$^{\alpha V1}$ morphants displayed normal heart tube asymmetry (Fig. 2M; see Table S3 in the supplementary material). Thus, selective knockdown of α*V* supported its presence in DFCs by phenocopying the heart laterality defect.

Given the prominent role of αV integrins in mammalian cell migration (Hynes, 2002), we asked whether αV might be required for DFC migration. DFCs were identified in gastrulating embryos at 80% E by utilizing *cas* (Kikuchi et al., 2001), *sox17* (Alexander and Stainier, 1999) or *ntl* (Amack and Yost, 2004) as markers (Fig. 3; see Fig. S4 in the supplementary material). Over 76% of uninjected embryos or embryos injected with α*V1miss* showed ovoid DFC clustering forming 5-6 tiers of cells from the margin (Fig. 3A,B). By contrast, when embryos were injected with α*V1*, α*V2* or α*VEI10*, 53-69% of α*V* morphant DFCs were confined to a linear domain that had occasional gaps (Fig. 3C-E). This mutant DFC phenotype was independent of the markers used to identify the cells (see Fig. S4 in the supplementary material) and it could be rescued by co-injection of *mαV* mRNA. For example, although only 17.6±6.3% (*n*=69) of α*V1* morphants showed an ovoidal wild-type DFC clustering pattern, 56.3±1.1% (*n*=23) of morphants co-injected with *mαV* mRNA demonstrated the wild-type pattern (see Table S4 in the supplementary material). Rescue by *mαV* mRNA was also observed in α*V2* morphants (Fig. 3F). Finally, DFC-selective, DFC$^{\alpha V1}$ morphants also exhibited DFC phenotypes similar to that of the α*V1*, α*V2* or α*VEI10* morphants (see Table S3 in the supplementary material). Thus, the loss of αV function during gastrulation appears to impair DFC migration but not specification.

## Integrin β1b is the likely partner for αV in dorsal forerunner cells

Of the several β subunits that can pair with αV (Bouvard et al., 2001), zebrafish express β*5*, β*6*, β*8* and multiple forms of β*1* (β*1a*, β*1b*, β*1b.1*, β*1b.2*) and β*3* (β*3a*, β*3b*) (Ablooglu et al., 2007; Julich et al., 2005; Julich et al., 2009; Mould et al., 2006; Thisse et al., 2001). Based on the reported spatial and temporal expression patterns of these β subunits and on overlapping expression patterns with α*V* during gastrulation, β*1b* (*itgb1b* – Zebrafish Information Network) and β*5* (*itgb5* - Zebrafish Information Network) appeared to be the only potential partners for α*V* in DFCs. Consequently, we examined their localization patterns at gastrulation to establish the identity of the potential αV partner in DFCs. Both β integrins showed distinct localization patterns at mid-gastrulation stages (Fig. 4A,B). For example, although β*1b* transcripts were mainly present in the embryonic axis at 80% E (Fig. 4A), β*5* transcripts were only present in the marginal cells and there was a gap in its expression field (Fig. 4B). When embryos were examined at 80% E for *cas* expression in DFCs and for integrin β subunit expression by double wholemount in situ hybridization (WISH), the gap in the β*5* expression field in the marginal cells overlapped the embryonic axis and only β*1b* was present in DFCs (Fig. 4C,D). Consequently, the binding partner for αV in DFCs might be β1b.

To study β1b function, a translation-blocking MO (β*1b1)* and a splice-inhibiting MO (β*1bE10*) were employed (see Fig. S5 in the supplementary material). After injection of either MO at the 1-4 cell stage, DFC markers were still expressed but there was a DFC mutant phenotype similar to that observed in α*V* morphants (Fig. 4E-H). Later in development at 32 hours post-fertilization (hpf), β*1b1* morphants had pericardial edema and showed shorter and undulated midlines associated with U-shaped somites (Fig. 4I,J). When 0.7 ng β*1b1* or 5 ng β*1bEI10* were delivered at the 1-4 cell stage, these morphants showed reduced left-sided location of the liver (see Table S2 in the supplementary material). At these MO doses, considerable numbers of β*1b1* morphants exhibited an absence of liver primordium and some β*1bEI10* morphants had situs inversus totalis. When both β*1b1* and β*1bEI10* were co-injected, no liver primordium was evident (see Table S2 in the supplementary material). These results suggested that pleiotropic phenotypes might be caused by midline defects (Biemar et al., 2001) or lack of endoderm (Alexander and Stainier, 1999; Kikuchi et al., 2000; Komada and Soriano, 1999). As β*1b* is deposited maternally (Ablooglu et al., 2007; Mould et al., 2006) and its zygotic expression is maintained exclusively in the developing midline during gastrulation (Fig. 4A) (Julich et al., 2005), knocking down of maternal β*1b* with β*1b1* MO could contribute pleiotropic defects. Consequently, we used a lower dose of β*1b1* (0.5 ng) to minimize possible pleiotropic defects. Under these conditions, β*1b1* alone did not significantly alter the asymmetric *spaw* expression pattern (Fig. 4L; see Table S2 in the supplementary material). However, when 0.5 ng β*1b1* and 5 ng β*1bEI10* were each co-injected, the severity of randomized *spaw* expression

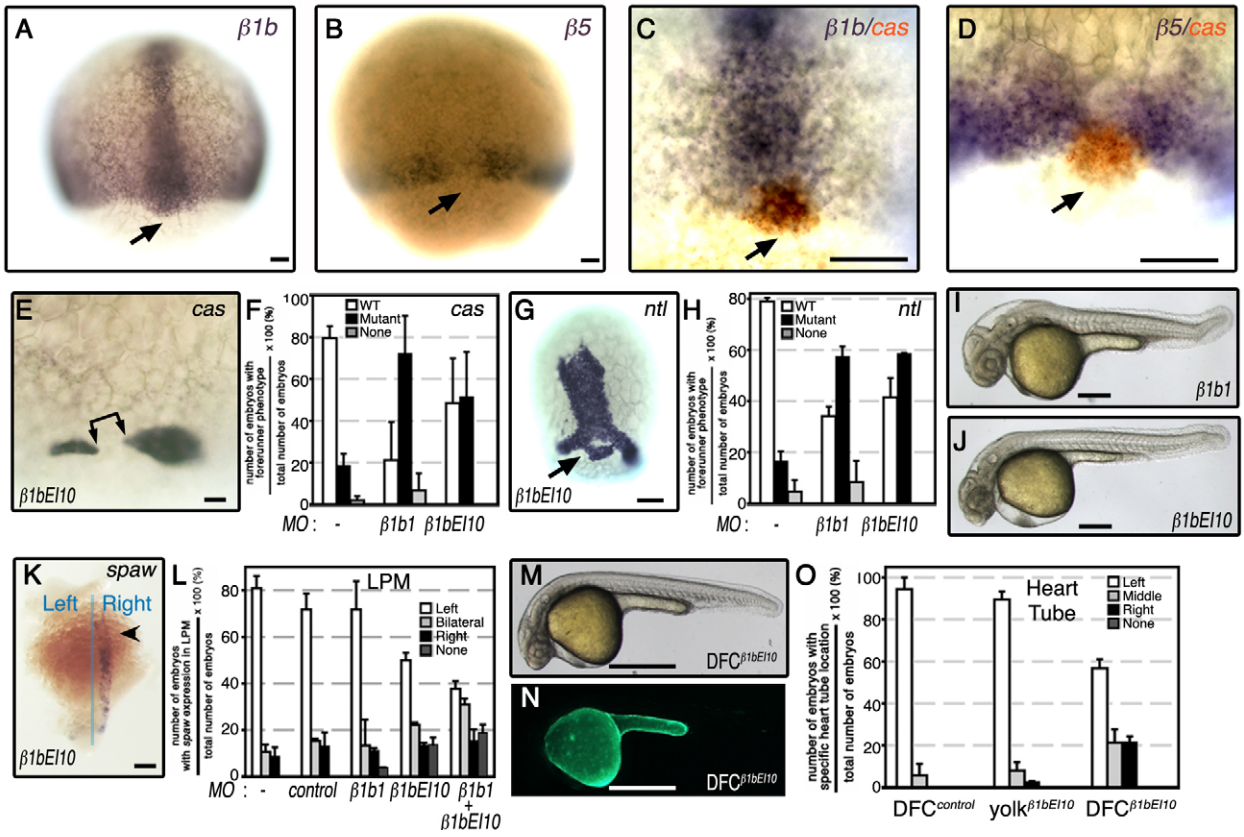


**Fig. 4. Integrin β*1b* morphants phenocopy the organ asymmetry defects of α*V* morphants.** (**A**,**B**) Dorsal views of wild-type embryos at 80% E, hybridized with a probe to β*1b* and β*5*. Putative DFCs are positive for β*1b* transcripts (black arrow; A), and β*5* transcripts are present in the marginal cells where there is a gap in this expression field (black arrow, B). (**C**,**D**) Double WISH samples showing simultaneous expression of *cas* (red orange) and β*1b* (dark purple; C); or *cas* (red orange) and β*5* (dark purple; D). (**E-H**) Dorsal views of embryos, slightly tilted to visualize *cas* (E) and *ntl* (G) expression in DFCs. Delivery of β*1b* MOs to 1- to 4-cell-stage embryos caused improper formation of forerunner cell cluster, assessed by *cas* (E) and *ntl* (G) expression in DFCs at 80% E. DFCs in β*1b* morphants had occasional gaps and were separated from the axis (black arrow in G). (F,H) Bar graphs summarize DFC phenotypes using *cas* or *ntl* as markers. Phenotypic classification of DFCs and data analyses were similar to those in Fig. 3. (**I**,**J**) β*1b* morphants developed undulated tail and abnormal head phenotype, which were evident at 32 hpf. (**K**) *spaw* expression in β*1b* morphants in lateral plate mesoderm (LPM) in 15-17 somite stage (SS) embryos. Dorsal view of a representative β*1bEI10* morphant (5 ng) showing right-sided *spaw* in LPM (arrowhead). (**L**) Bar graph showing the effects of β*1b* integrin loss-of-function on localization of *spaw* expression. (**M**) When β*1bEI10* was injected into yolk at mid-blastula stage (512-1000 cells), animals had wild-type phenotype. (**N**) A representative fluorescence image corresponding to M that shows MO presence only in the yolk cell. (**O**) Bar graph showing effects of β*1b* integrin loss selectively in DFCs on heart tube location. Data expressed are similar to those in Fig. 1E. Scale bars: 50 μm in A-D; 20 μm in E; 100 μm in G,K; 500 μm in I,J,M,N.

increased (Fig. 4K,L). In order to obtain more direct evidence for β1b function in DFCs, DFC-selective morphants (DFC$^{\beta 1bEI10}$) were generated by injecting β*1bEI10* into the yolk cell at the mid-blastula stage (Fig. 4M,N). The resulting DFC$^{\beta 1bEI10}$ morphants looked grossly similar to wild-type embryos (Fig. 4M versus Fig. 4J), but heart tube location was still randomized as with DFC$^{\alpha V1}$ morphants (Fig. 2M). By contrast, when β*1bEI10* was delivered to the yolk cell at dome stage to 30% E, these yolk $^{\beta 1bEI10}$ embryos showed normal heart tube asymmetry (Fig. 4O).

## αV and β1b genetically interact during DFC morphogenesis

Expression profiles and early tissue-specific knockdown phenotypes of α*V* and β*1b* indicated that development of proper body asymmetry requires their presence in DFCs. In order to examine possible α*V* and β*1b* genetic interaction, we used substantially lower doses of α*V1* (0.41 ng) or β*1bEI10* (1.1 ng) injections, to a level at which less then 15% embryos had an unclustered mutant DFC phenotype (see Fig. S6 and Table S5 in the supplementary material). However, co-injection of α*V1* and β*1bEI10* at these doses caused a dramatic increase in the frequency of the DFC clustering defect in embryos. Conversely, no such effect was observed when control α*V1miss* was co-injected with β*1bEI10*. These results are consistent with the idea that αV and β1b might interact in DFCs.

## α*V1* and β*1b* knockdown affects DFC orientation, shape and protrusive activity

As DFCs are migratory cells and WISH analysis of integrin morphants showed abnormal DFC clustering (Figs 3 and 4; see Fig. S4 in the supplementary material), we sought to identify possible migratory defects in DFCs by time-lapse imaging in *Tg(sox17:GFP)* transgenic fish (Mizoguchi et al., 2008) (Fig. 5). Migratory DFC progenitors in this transgenic line have been shown to intercalate mediolaterally and form a compact and oval-shaped DFC cluster at mid-gastrulation stages (Oteiza et al., 2008). We reasoned that either

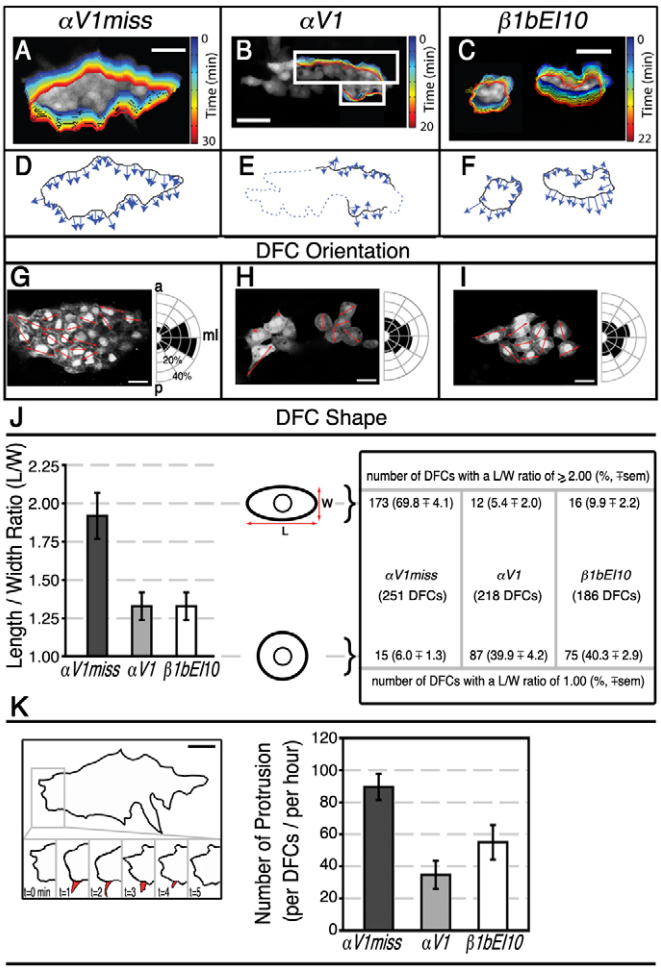


**Fig. 5. Effects of integrin α*V1* or β*1b* knockdown on DFC orientation, shape and protrusive activity.** At mid-gastrulation stages, DFCs show dynamic cellular protrusive activity and only control DFCs are normally mediolaterally oriented and have elongated morphology. (**A-C**) Dorsal views of *Tg(sox17:GFP)*-expressing embryos. Time-lapse images of migratory DFCs were collected by confocal microscopy at mid-gastrulation and migration was highlighted with pseudo-colors at one-minute intervals at the DFC cluster edge. Pseudo-colored outlines show the edges of DFC clusters at the timepoints indicated on the right. (A) At 70% E, all DFCs were clustered in α*V1miss* control embryos (1.75 ng; *n*=10) and remained clustered until the end of gastrulation (see also Movie 1 in the supplementary material). (B) Some DFCs in α*V1* morphants (1.25 ng; *n*=6) formed clusters (white rectangles). Later in development, cells outside of these clusters detached from each other (see also Movie 3 in the supplementary material). (C) β*1bEI10* (5 ng; *n*=6) morphants had multiple DFC clusters (see also Movie 5 in the supplementary material). (**D-F**) Pseudopod-like protrusion behavior of representative DFC cluster edges is shown between 4 to 5 minutes. Vectors illustrate the relative protrusion velocities of cells at the cluster edge and the direction of protrusions. Each vector represents a protrusion event, where its speed is proportional to the vector length. (D) Protrusions in α*V1miss* morphant DFCs formed towards the vegetal pole, whereas DFC protrusions in α*V1* (E) and β*1bEI10* morphants (F) lost their directionality. The relative locations of α*V1* morphant DFCs that did not form any clusters, or detached from each other later in development, are highlighted with dotted lines (E). (**G-I**) Representative ~3 μm thick focal plane confocal images of *Tg(sox17:GFP)*-expressing DFC clusters. Dorsal views of 80% E embryos are shown in all panels, anterior to the top. Half-rose diagrams show the angular distribution of the long axis of individual DFCs with respect to anterior-posterior (a,p) axis. Red arrows indicate the orientation of the long axis in each individual DFC that showed clear cellular boundary at these representative focal planes. Dividing DFCs (asterisks) were excluded from these measurements. ml, mediolateral axis. (**J**) The length (L) and width (W) measurements of individual DFCs were used to establish L-W ratios ± s.e.m. The majority of control α*V1miss*-injected embryos had a L-W ratio of 2.00, represented with ellipsoid cell shape. However, the L-W ratio in a significant fraction of morphant DFCs was close to 1.00, represented with circular cell shape. Total number of embryos and DFCs scored to determine individual cell orientation, length and width (L/W) ratios: 1.5 ng α*V1miss* (*n*=11, 251 DFCs); 1.25 ng α*V1* (*n*=11, 218 DFCs); 5 ng β*1bEI10* (*n*=11, 186 DFCs). (**K**) Average number of new and discrete large protrusions developed per DFC per hour were manually counted from the time-lapse confocal microscopy of migratory DFCs. DFC cluster edge in an α*V1miss*-injected embryo (see Movie 1 in the supplementary material) is outlined and a representative large protrusion is highlighted in red. The behavior and life span of the protrusions are shown below from 0-5 minutes. The bar graph shows the effects of αV and β1b knockdown on the number of protrusions formed per DFC per embryo per hour ± s.e.m. Total number of embryos studied: 1.5 ng α*V1miss* (*n*=5); 1.25 ng α*V1* (*n*=3); 5 ng β*1bEI10* (*n*=3). Scale bars: 50 μm in A-F; 20 μm G-I,K.

proliferation of DFC progenitors and/or motile properties and directionality of DFCs might be affected in α*V* and β*1b* integrin morphants. When examined at mid-gastrulation, both integrin morphants appeared to have numbers of DFCs comparable with control morphants: α*V1*, 38.9±9.5 cells/embryo (±s.d., *n*=19); β*1bEI10*, 39.2±8.6 (*n*=18); α*V1miss*, 37.9±9.5 (*n*=15). However, live imaging of DFCs in *Tg(sox17:GFP)* embryos revealed that α*V* or β*1b* morphants failed to form a single DFC cluster (Fig. 5B,C; see Movies 3-6 in the supplementary material), unlike α*V1miss*-injected embryos where DFCs formed an oval-shaped cluster that migrated towards the vegetal pole (Fig. 5A; see Movies 1 and 2 in the supplementary material). Furthermore, examination of DFC cluster edge protrusions and protrusion velocity maps (Fig. 5) revealed that both morphant DFCs exhibited disarrayed cluster edge protrusions (Fig. 5D-F).

To study the effect of integrin knockdown in individual DFCs in more detail, we evaluated DFC orientation, shape and the number of large and discrete protrusions per DFC in *Tg(sox17:GFP)* embryos. Although the majority (64.4±2.0%) of control DFCs aligned strongly to the mediolateral axis (e.g. between 60 and 120 degrees), only 46.6±3.7% of α*V1* and 41.4±4.5% of β*1bEI10* morphant DFCs did so (Fig. 5G-I), a significant difference compared with controls ($P \leq 0.0002$). Expressed another way, α*V1* and β*1b* morphant DFCs were oriented more randomly than control DFCs (ANOVA for anterior orientation, $P<0.014$; mediolateral orientation, $P<0.00015$; posterior orientation, $P<0.016$). Furthermore, individual control DFCs tended to be elongated, with a mean length-width ratio of 1.92±0.15, whereas integrin morphant DFCs tended to be rounder, with a mean length-width ratio of 1.33±0.09 ($P<0.0001$) (Fig. 5J). When large and discrete new protrusions in clustered or unclustered individual DFCs were tracked in time-lapse sequences, the average lifespan of protrusions was similar in controls and morphants (~4.6 minutes; ANOVA $P>0.10$). However, the number of protrusions formed by morphant DFCs was significantly reduced ($P \leq 0.02$; α*V1*, 34.7±8.7 protrusions

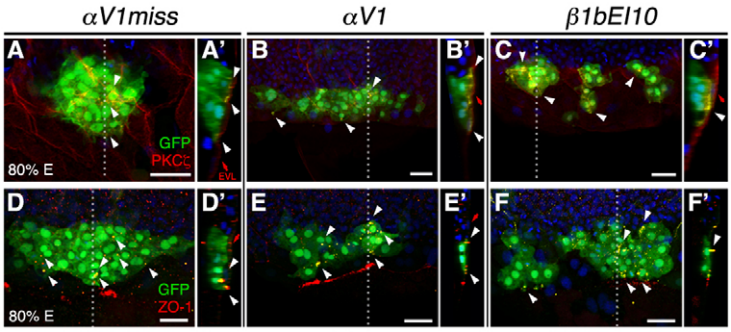


**Fig. 6. Apical attachment of DFC to EVL is maintained in αV and β1b morphants.** (**A-F'**) Confocal images of DFCs in *Tg(sox17:GFP)*-expressing embryos (green) nuclear-stained (blue) and immunolabeled with anti-aPKC-ζ antibody (red) (A-C) or with anti-ZO-1 antibody (red) (D-F); channels are merged. Dorsal views of 80% E embryos are shown in all panels, anterior to the top. Sagittal confocal sections at the position of the dotted lines are shown in A′ to F′, embryo surface to the right. Representative embryos that were injected with 1.5 ng α*V1miss* (A,D), 1.25 ng α*V1* (B,E), or 5 ng β*1bEI10* (C,F). (A-C) 3D rendering of multiple focal planes through the embryo at the level of DFCs. At 80% E, aPKC-ζ staining demarcates the DFC-EVL interface (A′-C′, white arrowheads). (D-F) Single dorsal focal planes of DFC clusters. Embryos were immunolabeled with ZO-1, which was enriched between DFCs and the interior surface of overlying EVL (D-F′, white arrowheads). Scale bars: 30 μm.

per embryo per hour; β*1bEI10*, 55.0±10.8; α*V1miss* control, 89.6±8.2; Fig. 5K). Thus, knockdown of α*V1* or β*1b* in DFCs appears to affect their orientation, shape and protrusive activity.

Although DFCs in α*V1* and β*1b* morphants showed morphologic and migratory defects, their vegetal migration did not seem to be affected, suggesting that αV and β1b might not be essential for this latter process. As earlier studies indicated that DFC and enveloping layer (EVL) attachments couple epiboly movements of both tissues towards the vegetal pole (D'Amico and Cooper, 1997; Oteiza et al., 2008; Solnica-Krezel et al., 1996), we examined DFC-EVL interactions. Confocal images of GFP(+) DFCs of *Tg(sox17:GFP)* morphants were examined by aPKC-ζ and ZO-1 immunolabeling. At 80% E, the DFC-EVL interface was enriched for tight junction components aPKC-ζ and ZO-1 in all three morphants (α*V1miss*, α*V1*, β*1bEI10*; Fig. 6). Thus, DFC-EVL connections in α*V* and β*1b* morphants are still maintained.

## Kupffer's vesicle development is disrupted in αV and β1b loss-of-function mutants

As migratory DFCs are precursors of KV (Cooper and D'Amico, 1996; D'Amico and Cooper, 1997; Essner et al., 2005; Melby et al., 1996), we reasoned that KV organogenesis might be affected by αV and β1b loss-of-function. Therefore, the physical dimensions of KV and the number of cilia per KV were determined (Fig. 7A-G). There was a strong positive correlation between KV volume and cilia number per KV, both in controls and in embryos in which α*V* and β*1b* had been knocked down ($r$=0.858; Fig. 7H). Compared with controls, both KV volume and cilia number per KV were significantly reduced in αV and β1b morphants (Fig. 7H). In uninjected embryos or those injected with control MO α*V1miss*, the mean number of cilia per KV was 38.5±3.4 and 36.8±4.9, respectively. However, in α*V* morphants (α*V1*, α*VEI10*, α*V2* MOs), cilia number per KV (±s.e.m.) was 17.7±4.1, 19.9±5.8 and

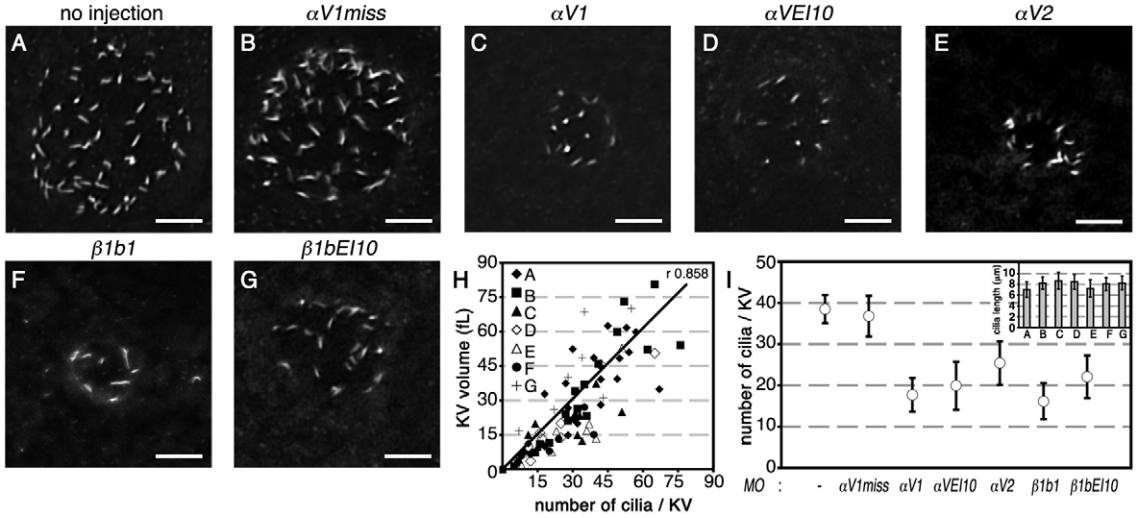


**Fig. 7. α*V* and β*1b* knockdown disrupts physical properties of Kupffer's vesicle.** (**A-G**) Dorsal views of 6-8 SS embryos; confocal images of Kupffer's vesicle (KV) cilia were detected by a fluorescent anti-acetylated tubulin antibody. Shown is a 3D rendering of multiple focal planes through the embryo at the level of KV. Total number of embryos used to determine number of cilia per KV and cilia length per morphant: uninjected (*n*=19); 1.75 ng α*V1miss* (*n*=16); 1.25 ng α*V1* (*n*=12); 5 ng α*VEI10* (*n*=9); 1.75 ng α*V2* (*n*=9); 1.0 ng β*1b1* (*n*=8); 5 ng β*1bEI10* (*n*=10). Scale bars: 20 μm. (**H**) Graphic representation of KV volume versus cilia number per KV. (**I**) Graphic representation of the number of cilia per KV in control and knockdown embryos. Inset, cilia length in α*V* and β*1b* morphants, indicated with their respective panel labels A to G. Data represent mean ± s.e.m.

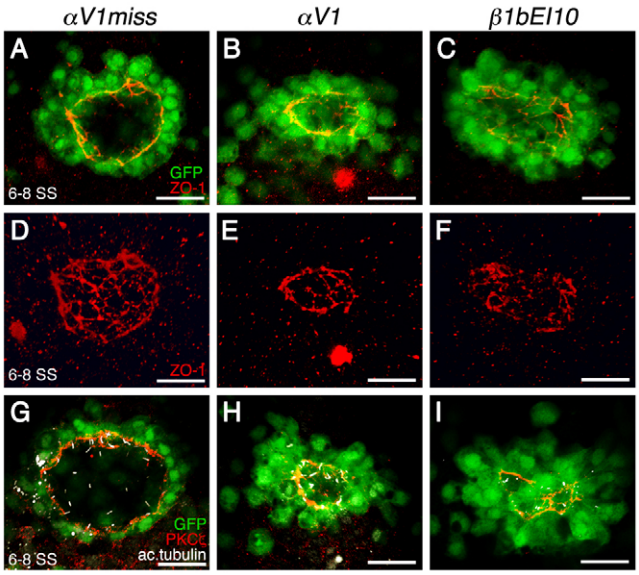


**Fig. 8. KV lumen does not properly form in αV and β1b morphants.** Confocal images of *Tg(sox17:GFP)*-expressing embryos (green) are shown. (**A-C**,**G-I**) Single focal planes at the center of the DFC cluster immunolabeled with anti-ZO-1 antibody (red; A-C) or anti-aPKC-ζ antibody (red) and anti-acetylated tubulin antibody (white; G-I). (**D-F**) 3D renderings of anti-ZO-1 labeled embryos of A-C. Dorsal views of 6-8 SS embryos are shown in all panels, anterior to the top. Embryos injected with α*V1miss* control MO developed a large fluid-filled lumen (A,G) that had a uniform ZO-1-labeled tight junction lattice within the DFC-derived lining of the KV (D). However, in α*V* (B,H) and β*1b* (C,I) morphants, DFCs did not aggregate properly, yielding a dysmorphic ZO-1 lattice (E,F). Anti-aPKCζ staining shows that KV cells in α*V1miss* morphants were polarized (G), but not in α*V* (H) and β*1b* morphants (I). Scale bars: 30 μm.

25.4±5.3, respectively, whereas in β*1b* morphants (β*1b1* or β*1bEI10* MOs) it was 16.2±4.4 and 22.1±5.2, respectively (Fig. 7I). Furthermore, because KV organogenesis could be uncoupled from KV ciliogenesis by disruption of non-canonical Wnt signaling to yield short cilia (Oishi et al., 2006), we also examined cilia length and determined that it was similar in all morphants (Fig. 7I, inset).

## DFC-to-KV organization is affected in integrin morphants

As both integrin mutants have fewer cilia in their KVs and apparent KV volume is reduced (see Fig. 8), we examined the DFC-to-KV organization process in more detail. In a recent study it was reported that KV ciliogenesis and lumen formation are directly coupled (Oteiza et al., 2008). When DFCs of control α*V1miss* morphants were examined at 6-8 somite stage (SS), GFP(+) cells in *Tg(sox17:GFP)* were connected with tight junctions that were localized in a single cell layer that formed the lining of a single fluid-filled KV lumen (Fig. 8A). However, neither α*V1* nor β*1bEI10* morphants developed such uniform tight junctions demarking a fluid-filled lumen within the GFP(+) cell cluster (Fig. 8B,C). Furthermore, although 3D renderings of ZO-1-labeled control embryos had a uniform tight junction lattice (Fig. 8D), DFCs in α*V1* and β*1bEI10* morphants failed to aggregate properly and yielded a dysmorphic ZO-1 lattice (Fig. 8E,F). Unlike in control embryos, GFP(+) DFCs were partially polarized in the integrin morphants and they displayed discontinuous or absent aPKC-ζ labeling and fewer cilia within DFC clusters (Fig. 8G-I). Overall, these observations suggest that body asymmetry defects in α*V* and β*1b* morphants originate from disrupted DFC organization and consequent KV malformation.

## DISCUSSION

Deletion of α*V* in mice causes early lethality at mid-gestation owing to placental defects; however, 20% of pups survive gestation with cerebral and intestinal blood vessel defects that contribute to their early demise (Bader et al., 1998). Lack of very early developmental defects in these animals could be attributed, in part, to maternally deposited αV protein (Sutherland et al., 1993). As depletion of both maternal and zygotic αV is difficult to achieve in mammalian models, the functional contribution of maternal αV cannot be inferred. By contrast, transient gene knockdown in zebrafish by injection of antisense MOs at the 1- to 4-cell stage could deplete zygotic transcripts and maternal transcripts not yet translated in the egg (Eisen and Smith, 2008; Nasevicius and Ekker, 2000). As zebrafish α*V* is deposited maternally like its murine counterpart and is expressed throughout gastrulation (Ablooglu et al., 2007), we used a series of MOs to determine the role of αV during early zebrafish development. Several new conclusions can be drawn from these studies. First, knockdown of α*V* in zebrafish leads to left-right asymmetry defects affecting multiple visceral organs, in addition to vascular defects previously described in αV knockout mice. Second, randomized visceral organ asymmetry in α*V* morphants could be explained by defective DFC migration and/or organization, leading to a malformed KV laterality organ. Third, the integrin β*1b* subunit is expressed in DFCs and its knockdown also causes a laterality phenotype. These results demonstrate a novel contribution of αV to early vertebrate development and suggest a previously unrecognized role for integrin αVβ1b within DFCs to form a normal KV, which in turn is essential for the establishment of proper left-right body asymmetry.

In preliminary work with α*V* MOs, we noticed altered heart tube asymmetry that could be partially rescued by injection of *m*α*V* mRNA (Fig. 1). As expression of left-sided genes (*spaw* and *lft2*) was randomized in α*V* morphants, the observed body asymmetry defects most likely did not originate from defective midline structures (Bisgrove et al., 2000). This was further supported by the observations that α*V* morphants had intact *ntl*-positive notochords and showed randomization of the normal left-right asymmetric locations of the liver and pancreas (see Fig. S2 in the supplementary material), features not characteristic of anterior midline defects (Bisgrove et al., 2000).

Given the generalized left-right asymmetry defects in α*V* morphants, we focused our attention on DFCs, which arise at the onset of gastrulation (Cooper and D'Amico, 1996; D'Amico and Cooper, 1997; Melby et al., 1996; Oteiza et al., 2008) and are precursors of KV (Amack et al., 2007; Amack and Yost, 2004; Essner et al., 2005; Essner et al., 2002; Oishi et al., 2006; Schneider et al., 2008). The robust early embryonic α*V* expression profile suggested that α*V* mRNA might be present in DFCs, and when we delivered α*V1* MO selectively into these cells by injecting into the yolk cell at mid-blastula stage, heart tube location was randomized (Fig. 2). Consequently, these data support an essential role for αV in DFCs and laterality specification. To identify a potential β partner for αV in DFCs, mRNA expression domains for several integrin β subunits were examined. Of these, only β*1b* transcripts were present in DFCs (Fig. 4). Moreover, when the locations of migratory DFCs were identified with multiple DFC markers (*cas*,

*ntl* and *sox17*), the selective knockdown of either αV or β*1b* resulted in the same DFC phenotype: a linear domain with occasional gaps, in contrast to ovoid DFC clusters in controls (Figs 3 and 4; see Fig. S4 in the supplementary material). Similar DFC mutant phenotypes have been reported in embryos with defective $Ca^{2+}$ fluxes in DFCs, and in $G_{\alpha 12}$ or $G_{\alpha 13a}$ morphants (Lin et al., 2009; Schneider et al., 2008). As αV and β*1b* morphant DFCs still express forerunner-specific markers, we posit that αV and β1b are not required for DFC specification. Migratory DFC progenitors normally intercalate mediolaterally and form an oval-shaped DFC cluster by mid-gastrulation (Oteiza et al., 2008). The unclustered and disoriented DFCs in integrin morphants suggest that αVβ1b is required for DFC migration and clustering.

It is interesting to note that the migratory defect seems to be specific for mediolateral DFC clustering but not for epiboly movements towards the vegetal pole because DFC-EVL connections that couple epiboly movements of both tissues towards the vegetal pole are still maintained in both morphants (Fig. 6). As the DFC-EVL connections allow a subset of DFCs to be pre-polarized, by having their apical contact with the overlying EVL (Oteiza et al., 2008), the maintenance of DFC-EVL connections in αV and β*1b* morphants allows us to assume the integrin αVβ1b is not essential for DFC polarization. However, because KVs in αV and β*1b* morphants formed a dysmorphic tight junction lattice that normally demarks the fluid-filled KV lumen (Fig. 8), integrin αVβ1b appears essential for DFC-to-KV organization. In addition, our studies do not exclude the possibility of further αVβ1b involvement in events later in KV development.

αVβ1 has not been studied extensively in mammals, in part because it is usually found in cells that express many different integrins, including other αV integrins, and because there is a dearth of αVβ1-specific antibodies and inhibitors. In addition to serving as a receptor for several RGD-containing matrix proteins (Hynes, 2002; Takada et al., 2007), αVβ1 serves as a receptor or co-receptor for several viruses, including adenovirus (Davison et al., 2001; Li et al., 2001), foot-and-mouth disease virus (Jackson et al., 2002), parechovirus (Triantafilou et al., 2000) and metapneumovirus (Cseke et al., 2009). Although many integrins function as both adhesion and signaling receptors (Hynes, 2002; Takada et al., 2007), the role of αVβ1 in cell signaling remains to be fully explored. Several in vitro studies have hinted at a role for αVβ1 in developmental processes. For example, αVβ1 has been implicated in adhesion and spreading of mouse embryonic cells on fibronectin (Yang and Hynes, 1996), migration and/or differentiation of rodent embryonic astrocytes and oligodendrocyte precursors (Milner et al., 1996; Milner et al., 2001), binding of chicken myotubes to agrin (Martin and Sanes, 1997) and cell binding to neural cell adhesion molecule L1 (Felding-Habermann et al., 1997). By taking advantage of the zebrafish system, the present study has uncovered a necessary role for αV and β1 during vertebrate gastrulation in regulating DFC migration, and DFC-to-KV organization that is essential for proper development of left-right asymmetry. Additional studies will be required to prove that αVβ1b is a heterodimer in DFCs, to identify the relevant matrix ligand(s) for αVβ1b during gastrulation and to determine if the signaling as well as the adhesive functions of this integrin are required for development of a proper KV.

**Acknowledgements**
We thank Drs N. Chi and D. Y. R. Stainier for providing *Tg(sox17:GFP)* fish, Oleg Tsivkovsk and Emerald Butko for technical assistance and the UCSD Fish Facility for maintaining zebrafish stocks. Confocal image analyses were done at the UCSD Neuroscience Microscopy Shared Facility (NIH P30 NS047101) and at the UCSD Cancer Center (NIH P30 CA23100). This work was supported by NIH grants F32 HL094012-01 to E.T. and HL78784 and HL56595 to S.J.S. Deposited in PMC for release after 12 months.

**Competing interests statement**
The authors declare no competing financial interests.

**Supplementary material**
Supplementary material for this article is available at
http://dev.biologists.org/lookup/suppl/doi:10.1242/dev.045310/-/DC1

**References**

**Ablooglu, A. J., Kang, J., Handin, R. I., Traver, D. and Shattil, S. J.** (2007). The zebrafish vitronectin receptor: characterization of integrin alphaV and beta3 expression patterns in early vertebrate development. *Dev. Dyn.* **236**, 2268-2276.
**Abrams, E. W. and Mullins, M. C.** (2009). Early zebrafish development: it's in the maternal genes. *Curr. Opin. Genet. Dev.* **19**, 396-403.
**Alexander, J. and Stainier, D. Y.** (1999). A molecular pathway leading to endoderm formation in zebrafish. *Curr. Biol.* **9**, 1147-1157.
**Amack, J. D. and Yost, H. J.** (2004). The T box transcription factor no tail in ciliated cells controls zebrafish left-right asymmetry. *Curr. Biol.* **14**, 685-690.
**Amack, J. D., Wang, X. and Yost, H. J.** (2007). Two T-box genes play independent and cooperative roles to regulate morphogenesis of ciliated Kupffer's vesicle in zebrafish. *Dev. Biol.* **310**, 196-210.
**Bader, B. L., Rayburn, H., Crowley, D. and Hynes, R. O.** (1998). Extensive vasculogenesis, angiogenesis, and organogenesis precede lethality in mice lacking all alpha v integrins. *Cell* **95**, 507-519.
**Biemar, F., Argenton, F., Schmidtke, R., Epperlein, S., Peers, B. and Driever, W.** (2001). Pancreas development in zebrafish: early dispersed appearance of endocrine hormone expressing cells and their convergence to form the definitive islet. *Dev. Biol.* **230**, 189-203.
**Bisgrove, B. W., Essner, J. J. and Yost, H. J.** (2000). Multiple pathways in the midline regulate concordant brain, heart and gut left-right asymmetry. *Development* **127**, 3567-3579.
**Bouvard, D., Brakebusch, C., Gustafsson, E., Aszodi, A., Bengtsson, T., Berna, A. and Fassler, R.** (2001). Functional consequences of integrin gene mutations in mice. *Circ. Res.* **89**, 211-223.
**Cochran, W. G.** (1977). *Sampling Techniques.* New York, NY: John Wiley and Sons.
**Cooper, M. S. and D'Amico, L. A.** (1996). A cluster of noninvoluting endocytic cells at the margin of the zebrafish blastoderm marks the site of embryonic shield formation. *Dev. Biol.* **180**, 184-198.
**Cseke, G., Maginnis, M. S., Cox, R. G., Tollefson, S. J., Podsiad, A. B., Wright, D. W., Dermody, T. S. and Williams, J. V.** (2009). Integrin alphavbeta1 promotes infection by human metapneumovirus. *Proc. Natl. Acad. Sci. USA* **106**, 1566-1571.
**D'Amico, L. A. and Cooper, M. S.** (1997). Spatially distinct domains of cell behavior in the zebrafish organizer region. *Biochem. Cell Biol.* **75**, 563-577.
**Davidson, L. A., Marsden, M., Keller, R. and Desimone, D. W.** (2006). Integrin alpha5beta1 and fibronectin regulate polarized cell protrusions required for *Xenopus* convergence and extension. *Curr. Biol.* **16**, 833-844.
**Davison, E., Kirby, I., Whitehouse, J., Hart, I., Marshall, J. F. and Santis, G.** (2001). Adenovirus type 5 uptake by lung adenocarcinoma cells in culture correlates with Ad5 fibre binding is mediated by alpha(v)beta1 integrin and can be modulated by changes in beta1 integrin function. *J. Gene Med.* **3**, 550-559.
**Delannet, M., Martin, F., Bossy, B., Cheresh, D. A., Reichardt, L. F. and Duband, J. L.** (1994). Specific roles of the alpha V beta 1, alpha V beta 3 and alpha V beta 5 integrins in avian neural crest cell adhesion and migration on vitronectin. *Development* **120**, 2687-2702.
**Eisen, J. S. and Smith, J. C.** (2008). Controlling morpholino experiments: don't stop making antisense. *Development* **135**, 1735-1743.
**Essner, J. J., Vogan, K. J., Wagner, M. K., Tabin, C. J., Yost, H. J. and Brueckner, M.** (2002). Conserved function for embryonic nodal cilia. *Nature* **418**, 37-38.
**Essner, J. J., Amack, J. D., Nyholm, M. K., Harris, E. B. and Yost, H. J.** (2005). Kupffer's vesicle is a ciliated organ of asymmetry in the zebrafish embryo that initiates left-right development of the brain, heart and gut. *Development* **132**, 1247-1260.
**Ezin, A. M., Skoglund, P. and Keller, R.** (2006). The presumptive floor plate (notoplate) induces behaviors associated with convergent extension in medial but not lateral neural plate cells of *Xenopus*. *Dev. Biol.* **300**, 670-686.
**Felding-Habermann, B., Silletti, S., Mei, F., Siu, C. H., Yip, P. M., Brooks, P. C., Cheresh, D. A., O'Toole, T. E., Ginsberg, M. H. and Montgomery, A. M.** (1997). A single immunoglobulin-like domain of the human neural cell adhesion molecule L1 supports adhesion by multiple vascular and platelet integrins. *J. Cell Biol.* **139**, 1567-1581.
**Hynes, R. O.** (2002). Integrins: bidirectional, allosteric signaling machines. *Cell* **110**, 673-687.

**Jackson, T., Mould, A. P., Sheppard, D. and King, A. M.** (2002). Integrin alphavbeta1 is a receptor for foot-and-mouth disease virus. *J. Virol.* **76**, 935-941.
**Julich, D., Geisler, R. and Holley, S. A.** (2005). Integrinalpha5 and delta/notch signaling have complementary spatiotemporal requirements during zebrafish somitogenesis. *Dev. Cell* **8**, 575-586.
**Julich, D., Mould, A. P., Koper, E. and Holley, S. A.** (2009). Control of extracellular matrix assembly along tissue boundaries via Integrin and Eph/Ephrin signaling. *Development* **136**, 2913-2921.
**Kikuchi, Y., Trinh, L. A., Reiter, J. F., Alexander, J., Yelon, D. and Stainier, D. Y.** (2000). The zebrafish bonnie and clyde gene encodes a Mix family homeodomain protein that regulates the generation of endodermal precursors. *Genes Dev.* **14**, 1279-1289.
**Kikuchi, Y., Agathon, A., Alexander, J., Thisse, C., Waldron, S., Yelon, D., Thisse, B. and Stainier, D. Y.** (2001). casanova encodes a novel Sox-related protein necessary and sufficient for early endoderm formation in zebrafish. *Genes Dev.* **15**, 1493-1505.
**Kimmel, C. B., Ballard, W. W., Kimmel, S. R., Ullmann, B. and Schilling, T. F.** (1995). Stages of embryonic development of the zebrafish. *Dev. Dyn.* **203**, 253-310.
**Komada, M. and Soriano, P.** (1999). Hrs, a FYVE finger protein localized to early endosomes, is implicated in vesicular traffic and required for ventral folding morphogenesis. *Genes Dev.* **13**, 1475-1485.
**Li, E., Brown, S. L., Stupack, D. G., Puente, X. S., Cheresh, D. A. and Nemerow, G. R.** (2001). Integrin alpha(v)beta1 is an adenovirus coreceptor. *J. Virol.* **75**, 5405-5409.
**Lin, F., Chen, S., Sepich, D. S., Panizzi, J. R., Clendenon, S. G., Marrs, J. A., Hamm, H. E. and Solnica-Krezel, L.** (2009). Galpha12/13 regulate epiboly by inhibiting E-cadherin activity and modulating the actin cytoskeleton. *J. Cell Biol.* **184**, 909-921.
**Long, S., Ahmad, N. and Rebagliati, M.** (2003). The zebrafish nodal-related gene southpaw is required for visceral and diencephalic left-right asymmetry. *Development* **130**, 2303-2316.
**Luo, B. H., Carman, C. V. and Springer, T. A.** (2007). Structural basis of integrin regulation and signaling. *Annu. Rev. Immunol.* **25**, 619-647.
**Machacek, M. and Danuser, G.** (2006). Morphodynamic profiling of protrusion phenotypes. *Biophys. J.* **90**, 1439-1452.
**Martin, P. T. and Sanes, J. R.** (1997). Integrins mediate adhesion to agrin and modulate agrin signaling. *Development* **124**, 3909-3917.
**McCarty, J. H., Monahan-Earley, R. A., Brown, L. F., Keller, M., Gerhardt, H., Rubin, K., Shani, M., Dvorak, H. F., Wolburg, H., Bader, B. L. et al.** (2002). Defective associations between blood vessels and brain parenchyma lead to cerebral hemorrhage in mice lacking alphav integrins. *Mol. Cell. Biol.* **22**, 7667-7677.
**McCarty, J. H., Lacy-Hulbert, A., Charest, A., Bronson, R. T., Crowley, D., Housman, D., Savill, J., Roes, J. and Hynes, R. O.** (2005). Selective ablation of alphav integrins in the central nervous system leads to cerebral hemorrhage, seizures, axonal degeneration and premature death. *Development* **132**, 165-176.
**Melby, A. E., Warga, R. M. and Kimmel, C. B.** (1996). Specification of cell fates at the dorsal margin of the zebrafish gastrula. *Development* **122**, 2225-2237.
**Milner, R., Edwards, G., Streuli, C. and Ffrench-Constant, C.** (1996). A role in migration for the alpha V beta 1 integrin expressed on oligodendrocyte precursors. *J. Neurosci.* **16**, 7240-7252.
**Milner, R., Relvas, J. B., Fawcett, J. and Ffrench-Constant, C.** (2001). Developmental regulation of alphav integrins produces functional changes in astrocyte behavior. *Mol. Cell. Neurosci.* **18**, 108-118.
**Mizoguchi, T., Verkade, H., Heath, J. K., Kuroiwa, A. and Kikuchi, Y.** (2008). Sdf1/Cxcr4 signaling controls the dorsal migration of endodermal cells during zebrafish gastrulation. *Development* **135**, 2521-2529.
**Mould, A. P., McLeish, J. A., Huxley-Jones, J., Gooonesinghe, A. C., Hurlstone, A. F., Boot-Handford, R. P. and Humphries, M. J.** (2006). Identification of multiple integrin beta1 homologs in zebrafish (*Danio rerio*). *BMC Cell Biol.* **7**, 24.
**Nasevicius, A. and Ekker, S. C.** (2000). Effective targeted gene 'knockdown' in zebrafish. *Nat. Genet.* **26**, 216-220.
**Nemeth, J. A., Nakada, M. T., Trikha, M., Lang, Z., Gordon, M. S., Jayson, G. C., Corringham, R., Prabhakar, U., Davis, H. M. and Beckman, R. A.** (2007). Alpha-v integrins as therapeutic targets in oncology. *Cancer Invest.* **25**, 632-646.
**Neugebauer, K. M., Emmett, C. J., Venstrom, K. A. and Reichardt, L. F.** (1991). Vitronectin and thrombospondin promote retinal neurite outgrowth: developmental regulation and role of integrins. *Neuron* **6**, 345-358.
**Ober, E. A., Field, H. A. and Stainier, D. Y.** (2003). From endoderm formation to liver and pancreas development in zebrafish. *Mech. Dev.* **120**, 5-18.
**Oishi, I., Kawakami, Y., Raya, A., Callol-Massot, C. and Izpisua Belmonte, J. C.** (2006). Regulation of primary cilia formation and left-right patterning in zebrafish by a noncanonical Wnt signaling mediator, duboraya. *Nat. Genet.* **38**, 1316-1322.
**Oteiza, P., Koppen, M., Concha, M. L. and Heisenberg, C. P.** (2008). Origin and shaping of the laterality organ in zebrafish. *Development* **135**, 2807-2813.
**Plow, E. F., Haas, T. A., Zhang, L., Loftus, J. and Smith, J. W.** (2000). Ligand binding to integrins. *J. Biol. Chem.* **275**, 21785-21788.
**Schneider, I., Houston, D. W., Rebagliati, M. R. and Slusarski, D. C.** (2008). Calcium fluxes in dorsal forerunner cells antagonize beta-catenin and alter left-right patterning. *Development* **135**, 75-84.
**Solnica-Krezel, L., Stemple, D. L., Mountcastle-Shah, E., Rangini, Z., Neuhauss, S. C., Malicki, J., Schier, A. F., Stainier, D. Y., Zwartkruis, F., Abdelilah, S. et al.** (1996). Mutations affecting cell fates and cellular rearrangements during gastrulation in zebrafish. *Development* **123**, 67-80.
**Sutherland, A. E., Calarco, P. G. and Damsky, C. H.** (1993). Developmental regulation of integrin expression at the time of implantation in the mouse embryo. *Development* **119**, 1175-1186.
**Takada, Y., Ye, X. and Simon, S.** (2007). The integrins. *Genome Biol.* **8**, 215.
**Testaz, S., Delannet, M. and Duband, J.** (1999). Adhesion and migration of avian neural crest cells on fibronectin require the cooperating activities of multiple integrins of the (beta)1 and (beta)3 families. *J. Cell Sci.* **112**, 4715-4728.
**Thisse, B., Pflumio, S., Fürthauer, M., Loppin, B., Heyer, V., Degrave, A., Woehl, R., Lux, A., Steffan, T., Charbonnier, X. Q. et al.** (2001). Expression of the zebrafish genome during embryogenesis (NIH R01 RR15402). ZFIN direct data submission. http://zfin.org.
**Thisse, B., Heyer, V., Lux, A., Alunni, V., Degrave, A., Seiliez, I., Kirchner, J., Parkhill, J. P. and Thisse, C.** (2004). Spatial and temporal expression of the zebrafish genome by large-scale in situ hybridization screening. *Methods Cell Biol.* **77**, 505-519.
**Triantafilou, K., Triantafilou, M., Takada, Y. and Fernandez, N.** (2000). Human parechovirus 1 utilizes integrins alphavbeta3 and alphavbeta1 as receptors. *J. Virol.* **74**, 5856-5862.
**Wendel, M., Sommarin, Y. and Heinegard, D.** (1998). Bone matrix proteins: isolation and characterization of a novel cell-binding keratan sulfate proteoglycan (osteoadherin) from bovine bone. *J. Cell Biol.* **141**, 839-847.
**Yamada, S., Brown, K. E. and Yamada, K. M.** (1995). Differential mRNA regulation of integrin subunits alpha V, beta 1, beta 3, and beta 5 during mouse embryonic organogenesis. *Cell Adhes. Commun.* **3**, 311-325.
**Yang, J. T. and Hynes, R. O.** (1996). Fibronectin receptor functions in embryonic cells deficient in alpha 5 beta 1 integrin can be replaced by alpha V integrins. *Mol. Biol. Cell* **7**, 1737-1748.

**Table S1. Analysis of heart tube location in αV morphants**

| Morpholino (MO) | | mRNA | $n_T$ | $n_{exp}$ | Left | Right | Middle | Absent |
|---|---|---|---|---|---|---|---|---|
| Uninjected | | – | 597 | 8 | 85.5±3.0% | 7.5±2.1% | 7.0±2.5% | 1.5±1.5% |
| 2.50 ng control MO | | – | 567 | 9 | 83.8±3.8% | 8.8±2.3% | 6.9±1.5% | 0.5±0.4% |
| 2.50 ng *αV1miss* | | – | 118 | 3 | 75.2±12.0% | 7.4±3.1% | 17.4±9.2% | 0% |
| None | | 200 pg *mαV* | 201 | 5 | 79.2±2.9% | 6.3±1.1% | 13.6±2.2% | 0% |
| 1.25 ng *αV1* | | – | 569 | 9 | 47.6±4.0% | 34.7±5.3% | 15.8±3.0% | 2.1±1.6% |
| 1.25 ng *αV1* | + | 200 pg *mαV* | 224 | 5 | 63.2±1.9% | 8.8±4.0% | 24.6±4.4% | 3.2±2.1% |
| 1.75 ng *αV2* | | – | 269 | 7 | 52.2±4.1% | 19.5±3.3% | 27.8±6.1% | 0.8±0.8% |
| 1.75 ng *αV2* | + | 200 pg *mαV* | 211 | 3 | 81.9±6.8% | 3.5±2.0% | 14.6±4.7% | 0% |

MOs and mRNAs were injected into 1- to 4-cell-stage wild-type embryos. Location of heart tube was examined with expression of *cmlc2* WISH at 26-28 hpf. Data were expressed as the number of embryos with a specific heart tube location divided by the total number of embryos used per experiment multiplied by 100 (%) ± s.e.m. $n_{exp}$=number of experimental repeats. $n_T$=total number of embryos.

**Table S2. Analysis of asymmetric molecular markers and location of visceral organs in αV and β1b morphants**

| Marker | Location | Morpholino | | mRNA | $n_T$ | $n_{exp}$ | Left | Right | Middle/Bilateral | Absent |
|---|---|---|---|---|---|---|---|---|---|---|
| *spaw* | LPM | Uninjected | | – | 163 | 4 | 80.9±5.3% | 8.6±3.9% | 10.6±3.2% | 0% |
| | | 5.00 ng control MO | | – | 51 | 2 | 71.7±6.9% | 13.0±5.9% | 15.3±1.0% | 0% |
| | | 1.50 ng *αV1miss* | | – | 23 | 2 | 67.8±12.2% | 21.1±1.1% | 11.1±11.1% | 0% |
| | | 1.25 ng *αV1* | | – | 50 | 3 | 42.7±3.3% | 42.5±1.0% | 11.8±1.0% | 3.0±3.0% |
| | | 5.00 ng *αVEI10* | | – | 156 | 6 | 51.9±3.4% | 13.4±4.9% | 28.2±2.5% | 6.5±3.4% |
| | | 0.50 ng *β1b1* | | – | 256 | 6 | 71.7±7.0% | 11.1±2.9% | 13.3±2.9% | 3.9±2.4% |
| | | 5.00 ng *β1bEI10* | | – | 118 | 5 | 49.9±8.6% | 13.4±3.3% | 22.3±5.2% | 13.7±4.2% |
| | | 5.00 ng *β1bEI10* + 0.50 ng *β1b1* | | – | 96 | 2 | 37.7±2.0% | 15.3±8.2% | 31.0±11.9% | 18.9±4.6% |
| *lft2* | heart | Uninjected | | – | 474 | 6 | 83.7±5.4% | 3.4±1.8% | 2.8±1.5% | 2.8±1.1% |
| | | 5.00 ng control MO | | – | 251 | 3 | 76.4±0.3% | 12.2±4.6% | 6.4±2.9% | 5.0±5.0% |
| | | 1.25 ng *αV1* | | – | 339 | 2 | 34.5±4.2% | 21.3±1.3% | 17.3±6.1% | 27.0±11.6% |
| | | 5.00 ng *αVEI10* | | – | 90 | 2 | 63.2±7.6% | 18.1±3.5% | 0% | 18.8±3.5% |
| | | 5.00 ng *β1bEI10* | | – | 68 | 2 | 65.7±12.7% | 13.7±9.8% | 2.0±2.0% | 15.7±7.8% |
| *vtn* | liver | Uninjected | | – | 499 | 8 | 82.4±2.0% | 6.9±1.2% | 10.4±1.9% | 0.2±0.2% |
| | | 2.50 ng control MO | | – | 351 | 5 | 85.9±4.7% | 11.6±4.5% | 2.1±1.1% | 0.4±0.3% |
| | | None | | 200 pg *mαV* | 122 | 3 | 72.8±3.1% | 12.8±4.0% | 11.8±4.4% | 2.6±1.3% |
| | | 1.25 ng *αV1* | | – | 616 | 10 | 46.5±3.3% | 30.5±3.4% | 11.0±2.2% | 12.0±2.5% |
| | | 1.25 ng *αV1* | + | 200 pg *mαV* | 211 | 6 | 63.6±6.5% | 18.0±2.1% | 8.5±3.1% | 9.9±4.2% |
| | | 1.75 ng *αV2* | | – | 84 | 3 | 45.2±9.3% | 14.0±7.0 % | 0% | 45.9±4.5% |
| | | 1.75 ng *αV2* | + | 200 pg *mαV* | 73 | 1 | 61.6% | 11.0% | 4.1% | 23.3% |
| | | 0.70 ng *β1b1* | | – | 182 | 4 | 38.4±11.4% | 14.6±5.7% | 8.2±3.4% | 38.8±15.6% |
| | | 5.00 ng *β1bEI10* | | – | 64 | 3 | 55.4±2.9% | 24.1±8.1% | 0% | 20.5±10.7% |
| | | 5.00 ng *β1bEI10* + 0.70 ng *β1b1* | | – | 53 | 3 | 1.9±1.9% | 0% | 0% | 98.1±1.9% |
| *pdx1* | pancreas | Uninjected | | – | 463 | 7 | 10.8±2.4% | 85.8±2.2% | 3.2±1.5% | 0.2±0.2% |
| | | 2.50 ng control MO | | – | 351 | 5 | 13.3±4.7% | 85.6±4.4% | 0.5±0.5% | 0.6±0.6% |
| | | None | | 200 pg *mαV* | 122 | 3 | 16.5±3.9% | 78.1±2.5% | 3.9±2.9% | 1.6±1.6% |
| | | 1.25 ng *αV1* | | – | 616 | 10 | 35.8±4.4% | 46.2±4.1% | 6.2±1.8% | 11.8±2.8% |
| | | 1.25 ng *αV1* | + | 200 pg *mαV* | 211 | 6 | 23.5±3.2% | 62.9±5.7% | 9.4±2.0% | 4.7±2.5% |
| | | 1.75 ng *αV2* | | – | 84 | 3 | 14.1±7.1% | 55.6±6.9% | 0% | 30.4±6.4% |
| | | 1.75 ng *αV2* | + | 200 pg *mαV* | 73 | 1 | 21.9% | 69.9% | 2.7% | 5.5% |

MOs and mRNAs were injected into 1- to 4-cell-stage wild-type embryos. Location of molecular markers or organ primordia was examined with WISH analysis. Data were expressed as the number of embryos with specific marker/organ location divided by the total number of embryos used per experiment multiplied by 100 (%) ± s.e.m. $n_{exp}$=number of experimental repeats. $n_T$=total number of embryos.

**Table S3. Analysis of heart tube and liver location in DFC-targeted integrin morphants**

| Marker | Marker location | Injection stage | Morpholino | $n_T$ | $n_{exp}$ | Left | Right | Middle | Absent |
|---|---|---|---|---|---|---|---|---|---|
| *cmlc2* | heart tube | 512-1000 cell | 2.50 ng control MO | 251 | 6 | 87.0±4.5% | 4.0±1.9% | 8.9±3.1% | 0% |
| | | | 5.00 ng control MO | 37 | 2 | 94.4±5.6% | 0% | 5.6±5.6% | 0% |
| | | | 1.25 ng *αV1* | 223 | 8 | 48.2±5.9% | 15.8±3.1% | 33.0±9.1% | 3.0±2.4% |
| | | | 5.00 ng *β1bEI10* | 125 | 3 | 56.7±4.3% | 21.6±2.6% | 21.2±6.4% | 0% |
| *cmlc2* | heart tube | Dome-30% epiboly | 1.25 ng *αV1* | 111 | 2 | 84.5±4.5% | 5.4±0.1% | 10.1±2.2% | 0% |
| | | | 5.00 ng *β1bEI10* | 147 | 2 | 89.5±3.8% | 2.6±0.2% | 7.9±4.0% | 0% |
| *vtn* | liver | 512-1000 cell | 2.50 ng control MO | 242 | 6 | 82.9±4.4% | 10.0±2.6% | 7.2±2.7% | 0% |
| | | | 1.25 ng *αV1* | 197 | 3 | 66.4±4.8% | 17.3±2.4% | 15.0±2.9% | 1.3±0.5% |

MOs were injected into yolk cells at indicated stages into wild-type embryos. Location of heart tube or liver was examined with WISH analysis. Data were expressed as the number of embryos with specific marker/organ location divided by the total number of embryos used per experiment multiplied by 100 (%) ± s.e.m. $n_{exp}$=number of experimental repeats. $n_T$=total number of embryos.

**Table S4. Analysis of migratory DFC phenotypes in integrin morphants at 80-90% epiboly**

| Marker | Injection stage | Morpholino | mRNA | $n_T$ | $n_{exp}$ | WT | Mutant | Absent |
|---|---|---|---|---|---|---|---|---|
| *cas* | 1 to 4 cell | Uninjected | – | 124 | 5 | 77.9±6.9% | 19.9±6.8% | 2.2±2.5% |
| | | 1.75 ng *αV1miss* | – | 51 | 2 | 75.7±6.1% | 17.1±4.0% | 7.1±10.1% |
| | | None | 200 pg *mαV* | 19 | 2 | 63.3±4.7% | 26.7±9.4% | 16.1±8.6% |
| | | 1.25 ng *αV1* | – | 69 | 4 | 17.6±6.3% | 69.3±9.5% | 13.2±7.3% |
| | | 1.25 ng *αV1* | 200 pg *mαV* | 23 | 2 | 56.3±1.1% | 43.7±1.1% | 0% |
| | | 1.75 ng *αV2* | – | 59 | 4 | 23.9±6.8% | 67.9±9.3% | 8.2±3.4% |
| | | 1.75 ng *αV2* | 200 pg *mαV* | 19 | 2 | 52.2±11.0% | 42.8±18.1% | 5.0±7.1% |
| | | 5.00 ng *αVEI10* | – | 23 | 2 | 47.3±15.5% | 52.7±15.5% | 0% |
| | | 0.75 ng *β1b1* | – | 40 | 3 | 21.1±18.3% | 72.2±18.0% | 6.7±8.2% |
| | | 5.00 ng *β1bEI10* | – | 23 | 2 | 48.5±21.4% | 51.5±21.4% | 0% |
| *sox17* | 1 to 4 cell | Uninjected | – | 53 | 3 | 68.8±7.5% | 22.9±7.9% | 8.3±4.8% |
| | | 1.75 ng *αV1miss* | – | 17 | 2 | 70.8±4.2% | 12.5±12.5% | 16.7±16.7% |
| | | 1.25 ng *αV1* | – | 27 | 2 | 19.2±4.2% | 53.3±13.3% | 27.5±19.2% |
| | | 1.75 ng *αV2* | – | 28 | 2 | 32.5±7.5% | 47.5±27.5% | 20.0±20.0% |
| | | 5.00 ng *αVEI10* | – | 12 | 1 | 58.3% | 33.3% | 8.3% |
| | | 0.75 ng *β1b1* | – | 18 | 2 | 37.0±8.4% | 33.1±24.0% | 29.9±15.6% |
| | | 5.00 ng *β1bEI10* | – | 21 | 1 | 38.1% | 47.6% | 14.3% |
| *ntl* | 1 to 4 cell | Uninjected | – | 42 | 3 | 79.0±1.4% | 16.5±3.9% | 4.5±4.5% |
| | | 1.75 ng *αV1miss* | – | 25 | 3 | 68.1±3.7% | 8.3±8.3% | 23.6±6.1% |
| | | 1.25 ng *αV1* | – | 53 | 4 | 29.2±7.6% | 60.9±2.0% | 9.9±5.8% |
| | | 5.00 ng *αVEI10* | – | 46 | 2 | 36.9±0.1% | 40.4±7.0% | 22.7±6.9% |
| | | 0.75 ng *β1b1* | – | 31 | 3 | 34.2±4.6% | 58.6±3.8% | 8.3±8.3% |
| | | 5.00 ng *β1bEI10* | – | 29 | 2 | 41.4±0.2% | 58.6±0.2% | 0% |
| *cas* | 512-1000 cell | Uninjected | – | 63 | 2 | 80.6±10.3% | 11.1±1.5% | 8.3±11.8% |
| | | 2. 50 ng *αV1miss* | – | 47 | 3 | 75.5±3.6% | 19.2±7.1% | 5.3 ±3.6% |
| | | 1.25 ng *αV1* | – | 48 | 3 | 36.8±5.3% | 41.5±8.8% | 21.7±3.8% |
| | | 1.75 ng *αV2* | – | 12 | 1 | 41.7% | 41.7% | 16.7% |
| | | 0.75 ng *β1b1* | – | 39 | 3 | 36.1±9.0% | 42.6±6.0% | 21.3±14.7% |
| | | 5.00 ng *β1bEI10* | – | 25 | 2 | 23.4±7.3% | 64.0±0.5% | 12.7±7.8% |

**Table S5. Low dose morpholino co-injections and analysis of migratory DFC phenotypes in integrin morphants at 80-90% epiboly**

| Marker | Injection stage | Morpholino | $n_T$ | $n_{exp}$ | WT | Mutant | Absent |
|---|---|---|---|---|---|---|---|
| *sox17* | 1 to 4 cell | 0.41 ng *αV1* | 227 | 4 | 84.9±3.7% | 13.1±4.7% | 2.0±1.1% |
| | | 1.5 ng *β1bEI10* | 156 | 4 | 83.9±2.5% | 14.8±2.0% | 1.3±1.3% |
| | | 0.41 ng *αV1miss* + 1.5 ng *β1bEI10* | 223 | 3 | 81.4± 5.0% | 18.1±5.2% | 0.5±0.5% |
| | | 0.41 ng *αV1* + 1.5 ng *β1bEI10* | 286 | 4 | 44.9±2.7% | 54.3±3.2% | 0.8±0.8% |

Location of DFCs was examined on live *Tg[sox17:eGFP]* embryos. Phenotypic classification of DFCs was as follows: WT, ovoid DFC marker expression domain; Mutant, a linear DFC marker expression domain with occasional gaps; Absent, no visible DFC marker expression. Data were expressed as the number of embryos with specific marker/organ location divided by the total number of embryos used per experiment multiplied by 100 (%) ± s.e.m. $n_{exp}$=number of experimental repeats. $n_T$=total number of embryos.